3D Conductive Polymer Printed Metasurface Antenna for Fresnel Focusing

designs

MDPI

Article

3D Conductive Polymer Printed Metasurface Antenna for Fresnel Focusing

Okan Yurduseven [1,*], Shengrong Ye [2], Thomas Fromenteze [3], Benjamin J. Wiley [4] and David R. Smith [5]

1 Institute of Electronics, Communications and Information Technology, School of Electronics, Electrical Engineering and Computer Science, Queen's University Belfast, Belfast BT3 9DT, UK
2 Multi3D Inc., 101-U Woodwinds Industrial Court, Cary, NC 27511, USA
3 XLIM Research Institute, University of Limoges, UMR 7252, F-87000 Limoges, France
4 Department of Chemistry, Duke University, Durham, NC 27708, USA
5 Department of Electrical and Computer Engineering, Center for Metamaterials and Integrated Plasmonics, Duke University, Durham, NC 27708, USA
* Correspondence: okan.yurduseven@qub.ac.uk

Received: 28 June 2019; Accepted: 2 September 2019; Published: 4 September 2019

Abstract: We demonstrate a 3D printed holographic metasurface antenna for beam-focusing applications at 10 GHz within the X-band frequency regime. The metasurface antenna is printed using a dual-material 3D printer leveraging a biodegradable conductive polymer material (Electrifi) to print the conductive parts and polylactic acid (PLA) to print the dielectric substrate. The entire metasurface antenna is 3D printed at once; no additional techniques, such as metal-plating and laser etching, are required. It is demonstrated that using the 3D printed conductive polymer metasurface, high-fidelity beam focusing can be achieved within the Fresnel region of the antenna. It is also shown that the material conductivity for 3D printing has a substantial effect on the radiation characteristics of the metasurface antenna.

Keywords: additive manufacturing; 3D printing; conductive polymer; microwaves; metamaterials; metasurface; beam-focusing; near-field; Fresnel

1. Introduction

Antennas with electromagnetic (EM) wavefront control capabilities offer unique opportunities with numerous applications in near-field (or Fresnel) [1–3] and far-field (or Fraunhofer) [4–6] beam-forming. The concept of Fresnel focusing enables the antenna radiated fields to be focused at a defined spot in the Fresnel region of the antenna, leading to increased field intensities at the focused region. This capability has been shown to hold significant potential in several emerging applications, such as near-field imaging [7], non-destructive testing [8], and wireless power transfer [9].

Conventionally, these antennas are created using printed-circuit-board (PCB) technology. In microwave and millimeter-wave frequency regimes, conventional fabrication techniques include photolithography or laser-based etching. Although high accuracy at extremely fine resolution limits can be achieved, these techniques can be limited in a number of key system metrics, such as exhibiting a rather complex fabrication process and requiring long prototyping times.

Recently, additive manufacturing (or 3D printing) of EM designs and antennas has gained traction as a means of offering rapid prototyping of EM structures [10–18]. In [10], a microstrip patch antenna operating at 7.5 GHz was fabricated using a fused filament technique to print the dielectric part and an ultrasonic wire mesh embedding technique for the conductor part. In [11], a 3D printed microwave variable phase shifter was presented, operating at 10 GHz frequency. The fabrication of

the phase shifter was achieved using a fused deposition modeling (FDM) additive manufacturing with copper electroplating. In [12], the design of a triple-mode circular waveguide horn antenna with corrugated chokes was presented for operation at a 7.40–7.89 GHz frequency band. The 3D fabrication of the antenna was achieved using a polycarbonate/acrylonitrile butadiene styrene (PC-ABS) material coated with conductive silver ink. In [13], a Fresnel zone plate lens was fabricated using an FDM MakerBot® Replicator® 2X (MakerBot Industries LLC, New York City, NY, USA) with a PREPERM® TP20280 (Premix OY, Rajamäki, Finland) 3D printing filament. The lens effect was achieved by varying the filling factor of the material, resulting in various relative permittivity values across the lens surface. Because this structure does not rely on guiding the electromagnetic (EM) waves using conductive walls, but rather on achieving the appropriate permittivity distribution to obtain the desired wavefront, no metallization was applied for the presented design. Another interesting application of using 3D printing for microwave devices was demonstrated in [14]. It was shown that using the same MakerBot® Replicator™ 2X as in [13], 3D printed dielectric substrates could be combined with commercial laminates to achieve a wide range of permittivities. As a continuation of research efforts on 3D printing lenses, in [15] a plano-concave shaped lens featuring negative-index characteristics was 3D printed for a 10–12 GHz frequency band of operation. The fabrication of the lens was achieved using commercial layered prototyping equipment (Objet Connex500). In [17], the authors presented a 3D printed compressive antenna architecture for computational radar imaging at K-band frequencies, 17.5–26.5 GHz. As a testament to the frequency scalability of the 3D printing concept to higher frequencies, such as millimeter-waves (30–300 GHz) and even THz waves (above 300 GHz), the design of various EM components from lenses to waveguides and antennas at such frequencies was demonstrated in [17,18].

A major limitation with conventional 3D printing techniques for EM structures that require conductive walls is the multi-step fabrication procedure required to fabricate such structures. 3D printing a volumetric antenna structure typically requires an electroplating technique or additional conductive coating techniques, resulting in a rather complicated and time-consuming fabrication campaign. Moreover, such techniques are extremely difficult to apply when fabricating designs that exhibit complex design features, such as structures that consist of subwavelength elements. In this paper, we demonstrate a 3D printed metasurface antenna for Fresnel focusing. The metasurface layer of the antenna is made of a biodegradable conductive polymer material, Electrifi, printed on a polylactic acid (PLA) dielectric substrate. Electrifi is the brand name of a conductive filament for fused filament fabrication (FFF) 3D printers manufactured by Multi3D (Multi 3D Inc, Cary, NC, USA) [19]. It is a metal-filled conductive polymer composite that consists primarily of biodegradable polyester and copper [20–24]. The conductive Electrifi material can easily be printed using the FFF technology. As opposed to conventional 3D printing methods, we demonstrate that the proposed 3D printing technique enables the antenna to be fabricated at once, circumventing the requirement for metal plating techniques, which can pose difficulties in plating complex structures. As the 3D printed conductive and dielectric layers of the proposed antenna are fully integrated during the printing process, no additional assembly methods are needed. To the best of our knowledge, the presented 3D printed metasurface antenna design is the first one where a microwave near-field focusing metasurface is obtained using a single-step, conductive/dielectric 3D printing procedure. The presented technology also paves the way for innovative antenna architectures, such as 3D printed conformal metamaterial antennas, which can find applications in remote sensing and 5G networks.

2. Materials and Methods

The 3D printed Fresnel focusing metasurface antenna is shown in Figure 1. The design consists of a PLA substrate (ε_r = 3 and tanδ = 0.02) sandwiched in between the metasurface layer on top and a ground plane at the bottom, both of which are printed using Electrifi. The metasurface layer is patterned into an array of subwavelength slot-shaped metamaterial elements (or meta-elements). These meta-elements couple to the guided mode (or the reference wave) launched into the PLA substrate

by a coaxial feed placed in the center of the antenna. The meta-elements are $\lambda_g/3$ long and $\lambda_g/10$ wide, where λ_g is the guided wavelength within the dielectric at 10 GHz, 1.73 cm. The aperture of the antenna is discretized into a regular grid of square pixels of $\lambda_g/2.5$ size, corresponding to $\lambda_0/4.3$ in free space, smaller than the periodicity of radiating elements in conventional array antennas ($\lambda_0/2$).

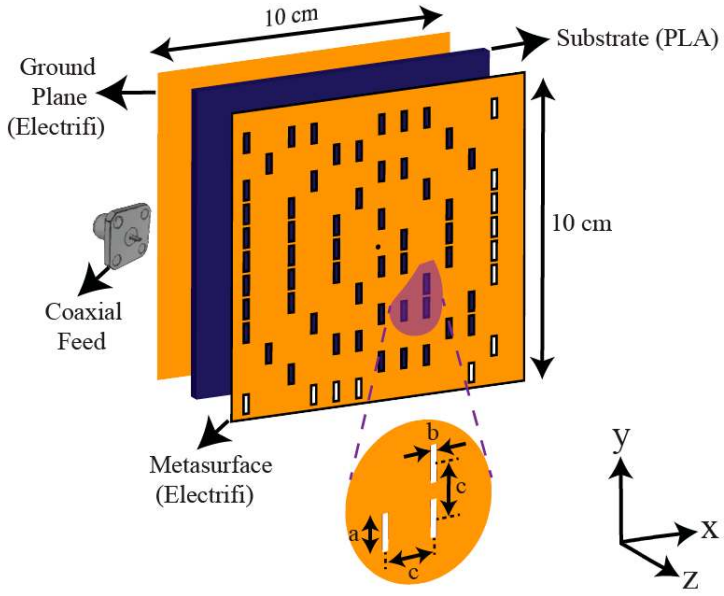

Figure 1. Depiction of a 3D printed holographic metasurface antenna for Fresnel focusing. Layers are shown separated for illustration. Meta-element dimensions are as follows: $a = \lambda_g/3$, $b = \lambda_g/10$, and $c = \lambda_g/2.5$, where the guided wavelength, λ_g, is 1.73 cm.

The PLA substrate is t_s = 3 mm thick, forming a 3D volumetric structure while ensuring the rigidity of the antenna and enabling single-mode operation, $t < \lambda_g/2$. The Electrifi metasurface layer and the ground plane are t_e = 0.4 mm thick, larger than the skin depth of the material at 10 GHz, δ = 38.9 µm. The 3D model files of the metasurface antennas studied in this paper are available as Supplementary Materials.

Focusing at an arbitrarily selected point in the Fresnel region requires that the wavefront within each discretized pixel on the aperture adds up constructively at the focal point. Therefore, to achieve Fresnel focusing, the guided-mode reference is modulated by the metasurface layer to result in the desired field distribution on the antenna aperture that produces the focus of interest [5]. This suggests that the metasurface layer acts as a holographic modulator, producing the focused beam when illuminated by the guided-mode reference wave. In this work, we make use of a binary modulation scheme, which involves treating the focal point as a virtual point source back-propagated to the aperture of the antenna and placing the meta-elements only at the points where the phase difference between the back-propagated aperture field and the guided-mode reference remains below a certain threshold. In this work, the optimum phase threshold was found to be ±60°. Increasing the phase threshold beyond this level increases the number of meta-elements in the metasurface layer, resulting in a stronger radiation from the antenna at the expense of increasing the sidelobe levels (worsening constructive interference). Reducing this phase threshold, on the other hand, reduces the number of meta-elements, and therefore the radiation from the antenna.

In Figure 2, we present the holographic beam-focusing concept using the 3D printed metasurface antenna. The first step in this process consists of determining the virtual point source at the position where the desired beam focusing is with the position of the point source being $\mathbf{r}\prime$ in Figure 2. The virtual point source is then back-propagated to the aperture of the antenna, $\mathbf{P} = e^{-jk|\mathbf{r}-\mathbf{r}\prime|}$ (amplitude dependency is dropped as beam fidelity is mainly controlled by phase information), producing a desired field distribution, $\mathbf{P}$, that focuses at the position of the virtual point source when radiated by the metasurface

antenna with the coordinates of the antenna being **r** in Figure 2. The second step in the design process is to design a metasurface layer that produces **P** when excited by the magnetic field of the reference wave launched by the coaxial feed, $\mathbf{H} = H_0^{(1)}(k_g \mathbf{r}) \sin\phi$. Here, k_g is the wavenumber within the substrate, $H_0^{(1)}$ is the Hankel function (zeroth order and first kind) and we consider only the y-component of the launched magnetic field exciting the slots with their longitudinal axes oriented along the y-axis. From this definition, the metasurface can be considered a phase grating, $\mathbf{M} = \mathbf{P}\mathbf{H}^{\dagger}$, where the symbol † denotes the complex conjugate operation. It should be noted that due to the linearly polarized coupling response of the slot-shaped meta-elements to the guided-mode reference along the y-axis, we consider a single-polarization case, suggesting that the fields are scalar, and use the bold font to denote the vector-matrix notation.

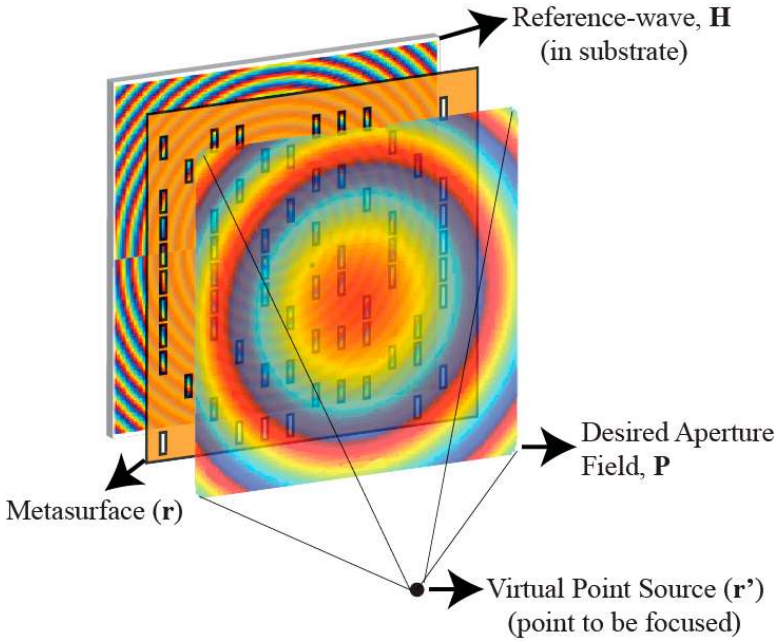

Figure 2. Depiction of the holographic beam-forming process.

The Electrifi conductive filament is a copper–polyester composite filament which has a conductivity of $\sigma = 1.67 \times 10^4$ S/m. The design of our 3D printer is based on an open source FFF D-Bot printer [25,26]. The original design was converted from a single Bowden extruder to a dual direct-drive extruder. Details on this modification process of the D-Bot 3D printer can be found in [20]. As a result, the 3D printer is capable of printing both the Electrifi and the PLA materials simultaneously. The nozzle size for printing is 0.5 mm and the print speed is 15 mm/s for Electrifi and 30 mm/s for PLA. The printing temperature for the Electrifi material is 140 °C, whereas the PLA material is printed at 190 °C. To print the Electrifi material, no heated bed is used, enabling us to maintain the maximum conductivity of the Electrifi material.

In this paper, we investigate Fresnel focusing for two different scenarios, namely, on-axis and off-axis. From antenna theory [27], the far-field limit of the designed aperture is calculated as $z_{max} = 0.66$ m, with the focal points selected to be $F_1(x = 0$ m, $y = 0$ m, $z = 0.2$ m) and $F_2(x = -0.05$ m, $y = 0.05$ m, $z = 0.2$ m), respectively. Here, F_1 denotes the on-axis focusing scenario, where the focusing is achieved along the broadside direction of the antenna (z-axis), whereas F_2 denotes the off-axis focusing scenario. The 3D printed metasurface antennas for the investigated focusing cases are shown in Figure 3.

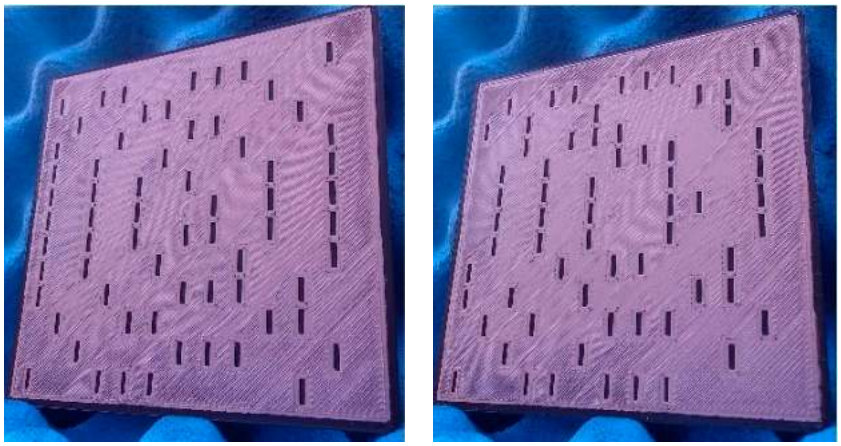

(**a**) (**b**)

Figure 3. 3D printed conductive polymer metasurface antennas for on-axis and off-axis Fresnel focusing: (**a**) on-axis focusing, $F_1(x = 0$ m, $y = 0$ m, $z = 0.2$ m) and (**b**) off-axis focusing, $F_2(x = -0.05$ m, $y = 0.05$ m, $z = 0.2$ m).

As shown in Figure 3, the distribution of the meta-elements in the metasurface layer changes as the focal point is varied. This is expected as the fields back-propagated from F_1 and F_2 to the antenna aperture are different, producing a different hologram pattern when interacted with the guided-mode reference. It should be noted that the connection between the ground plane and the coaxial connector was achieved using a silver paste to minimize the contact resistance between the two surfaces.

3. Results and Discussion

Following the fabrication of the metasurface antennas, the surface roughness of the finished prototypes shown in Figure 3 was measured using a Bruker Dektak 150 surface profilometer (Bruker, Billerica, MA, USA) [28] and was recorded to be 22 μm.

To characterize the fields radiated by the antennas at the focal distance, we used a near-field scanning system (NSI-200v-3x3, NSI, Torrance, CA, USA) [29–31]. Due to the scalar approximation of the problem at hand, the near-field characterization process was carried out to measure the electric field (E-field) polarized along the x-axis. The x-polarized E-field was radiated by the vertically oriented slot-shaped meta-elements coupling to the magnetic field of the guided mode along the y-axis. The measured E-field patterns at $z = 0.2$ m plane are shown in Figure 4, where the on-axis and off-axis focused beams are evident. To analyze the measured focusing fidelity, we compared the coordinates of the E-field intensity maxima in the cross-range plane (xy-plane) between the analytical and measured F_1 and F_2 values, and found an excellent agreement between them, that is, analytical $F_1(x = 0$ m, $y = 0$ m) compared to measured $F_1(x = 0$ m, $y = 0$ m), and analytical $F_2(x = -0.05$ m, $y = 0.05$ m) compared to measured $F_2(x = -0.048$ m, $y = 0.051$ m). It should be noted that, for this demonstration, the F_1 and F_2 focal points were chosen on an arbitrary basis and that the metasurface can focus at another desired point of interest within the Fresnel zone of the antenna aperture.

An important parameter to assess the focusing capabilities of the 3D printed metasurface antennas is the beam-waist diameter of the E-field patterns at the focal plane, $z = 0.2$ m. Analyzing the measured E-field patterns shown in Figure 4, the −3 dB full-width-half-maximum (FWHM) beam-waist values are calculated to be 6.82 cm for on-axis and 7.48 cm for off-axis focusing scenarios, respectively. These values are in good agreement with the theoretical beam-waist values, which are calculated to be 6.48 cm for on-axis and 6.89 cm for off-axis focusing scenarios, respectively [9]. We note that for the calculation of the theoretical beam-waist values, the Gaussian optics limits presented in [9] (which conventionally take $1/e^2$ width level as a reference) were converted to an FWHM scale, which is a more common metric in the antenna community.

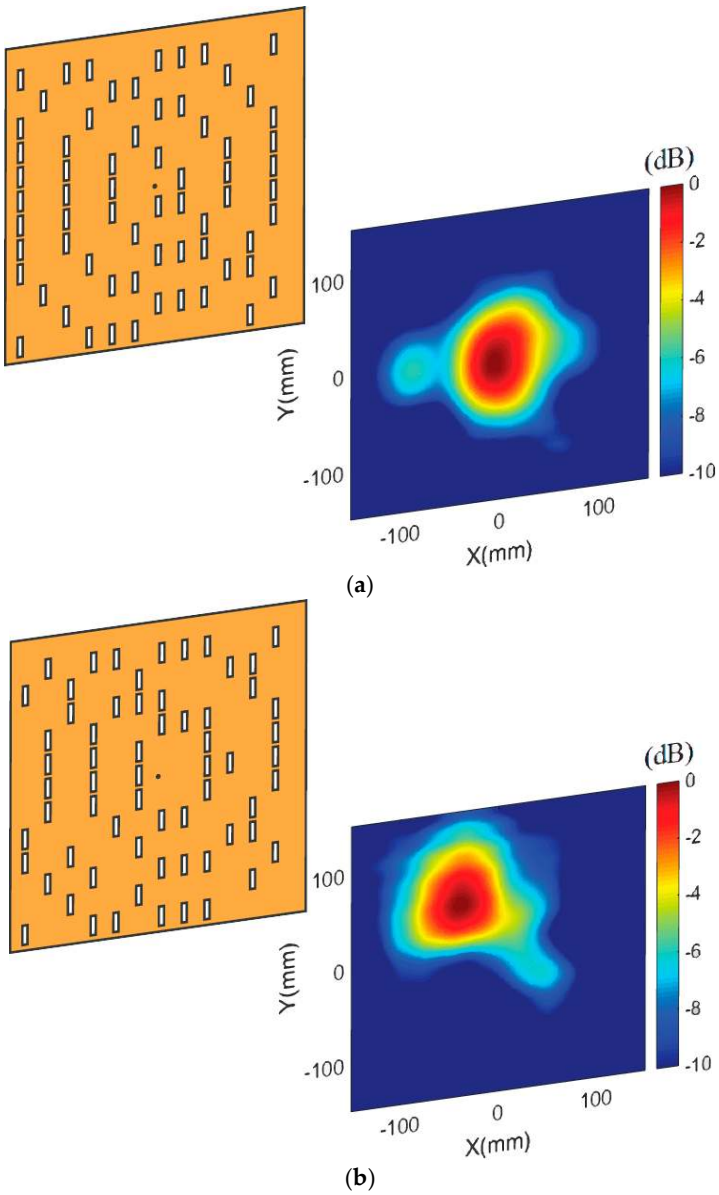

Figure 4. Measured E-field patterns at the focal plane, z = 0.2 m for (**a**) on-axis focusing and (**b**) off-axis focusing.

Conventionally, an antenna is designed for far-field operation. Analyzing antennas in the far-field is a well-defined problem with certain metrics used for performance evaluation, including antenna gain, sidelobe level, and -3 dB half-power-beamwidth (HPBW). In the near-field, however, the radiation pattern cannot be considered in its conventional far-field sense due to the presence of angular dependency with distance. However, to analyze the effect of the material conductivity on the antenna performance, we can use the relative change in these parameters as a function of varying material conductivity. To this end, we varied the conductivity of the Electrifi material within the range of $\sigma_{min} = 1.67 \times 10^3$ S/m and $\sigma_{max} = 1.67 \times 10^5$ S/m, and analyzed the conductivity dependency of the gain, sidelobe level, and HPBW values of the metasurface antenna in Table 1. This analysis was performed using a full-wave EM simulator, CST Microwave Studio (Dassault Systemes Simulia, Johnston, RI, USA), with lossy (tanδ = 0.02) and lossless (tanδ = 0) PLA material as the substrate. We also analyzed the polarization characteristics of the radiated fields by the slot-shaped meta-elements, which were measured to be above 40 dB due to the high aspect ratio of the slot-shaped geometry, exhibiting a strong, linearly polarized coupling response to the guided mode.

Table 1. Antenna performance as a function of material conductivity and dielectric loss.

PLA Substrate Loss (tanδ)	Material Conductivity (S/m)	Gain (dBi)	Sidelobe Level (dB)	HPBW (Degrees)
0 (lossless)	1.67×10^3	1.33	−11.4	22.4
	1.67×10^4	7.29	−13.2	20.4
	1.67×10^5	11	−13.6	18.9
0.02	1.67×10^3	0.34	−11.3	23.2
	1.67×10^4	5.31	−13.1	21.1
	1.67×10^5	7.55	−15	20.1

Several important conclusions can be drawn from Table 1. First, increasing the Electrifi material conductivity significantly increases the gain of the antenna. As an example, increasing the material conductivity from $\sigma = 1.67 \times 10^3$ S/m to $\sigma = 1.67 \times 10^5$ S/m, the gain is increased by 9.67 dB and 7.21 dB for the lossless and lossy PLA substrate scenarios, respectively. Second, albeit being limited in comparison to the effect of the material conductivity, the dielectric loss of the PLA material has a considerable effect on the gain performance of the antenna. Taking the actual conductivity of the Electrifi material as a reference, $\sigma = 1.67 \times 10^4$ S/m, the dielectric loss of the PLA substrate is responsible for a 1.98 dB difference in the gain value. Third, increasing the dielectric loss of the substrate reduces the sidelobe levels while widening the HPBW. This is expected because increasing the loss of the PLA substrate has a similar effect to truncating the aperture, resulting in a smaller effective aperture size. Fourth, and finally, as the material conductivity is increased, the sidelobe levels improve while the HPBW becomes narrower.

4. Conclusions

For this study, we demonstrated a 3D printed conductive polymer metasurface antenna for Fresnel focusing applications. Using the proposed antenna, high-fidelity beam focusing at arbitrarily selected focal points in the near-field zone of the antenna was achieved. It was also observed that improving the material conductivity could significantly enhance the radiation characteristics of the proposed antenna. While the 3D printing biodegradable Electrifi material used in this design has an electrical conductivity of $\sigma = 1.67 \times 10^4$ S/m, our ongoing studies suggest that a conductivity increase of 10 times can be achieved by increasing the amount of the copper in Electrifi. The proposed conductive polymer metasurface antenna is low-cost, simple to manufacture, and suitable for rapid prototyping. It can find applications in near-field imaging, non-destructive testing, and wireless power transfer, where rapid prototyping can be a significant advantage in the design process.

Supplementary Materials: The following are available online at http://www.mdpi.com/2411-9660/3/3/46/s1, File S1: Electrifi_3D_Model.

Author Contributions: Conceptualization, data curation, methodology, investigation, formal analysis, validation, writing—original draft preparation, writing—review and editing, O.Y.; conceptualization, methodology, investigation, writing—review and editing, S.Y.; investigation, formal analysis, writing—review and editing, T.F.; project administration, supervision, writing—review and editing, B.J.W.; project administration, supervision, funding acquisition, writing—review and editing, D.R.S.

Funding: This work was supported by the Air Force Office of Scientific Research (AFOSR, Grant No. FA9550-12-1-0491).

Conflicts of Interest: The authors declare no conflict of interest.

References

1. Ettorre, M.; Casaletti, M.; Valerio, G.; Sauleau, R.; Le Coq, L.; Pavone, S.C.; Albani, M. On the Near-Field Shaping and Focusing Capability of a Radial Line Slot Array. *IEEE Trans. Antennas Propag.* **2014**, *62*, 1991–1999. [CrossRef]
2. Martinez-Ros, A.J.; Gómez-Tornero, J.L.; Losada, V.; Mesa, F.; Medina, F. Non-Uniform Sinusoidally Modulated Half-Mode Leaky-Wave Lines for Near-Field Focusing Pattern Synthesis. *IEEE Trans. Antennas Propag.* **2015**, *63*, 1022–1031. [CrossRef]

3. Blanco, D.; Gómez-Tornero, J.L.; Rajo-Iglesias, E.; Llombart, N. Radially Polarized Annular-Slot Leaky-Wave Antenna for Three-Dimensional Near-Field Microwave Focusing. *IEEE Antennas Wirel. Propag. Lett.* **2014**, *13*, 583–586. [CrossRef]
4. Epstein, A.; Eleftheriades, G.V. Passive Lossless Huygens Metasurfaces for Conversion of Arbitrary Source Field to Directive Radiation. *IEEE Trans. Antennas Propag.* **2014**, *62*, 5680–5695. [CrossRef]
5. Yurduseven, O.; Marks, D.L.; Fromenteze, T.; Smith, D.R. Dynamically reconfigurable holographic metasurface aperture for a Mills-Cross monochromatic microwave camera. *Opt. Express* **2018**, *26*, 5281–5291. [CrossRef] [PubMed]
6. Johnson, M.C.; Brunton, S.L.; Kundtz, N.B.; Kutz, J.N. Sidelobe Canceling for Reconfigurable Holographic Metamaterial Antenna. *IEEE Trans. Antennas Propag.* **2015**, *63*, 1881–1886. [CrossRef]
7. Yurduseven, O.; Marks, D.L.; Fromenteze, T.; Gollub, J.N.; Smith, D.R. Millimeter-wave spotlight imager using dynamic holographic metasurface antennas. *Opt. Express* **2017**, *25*, 18230. [CrossRef] [PubMed]
8. Ziehm, C.; Hantscher, S.; Hinken, J.; Ziep, C.; Richter, M. Near field focusing for nondestructive microwave testing at 24 GHz–Theory and experimental verification. *Case Stud. Nondestruct. Test. Eval.* **2016**, *6*, 70–78. [CrossRef]
9. Smith, D.R.; Gowda, V.R.; Yurduseven, O.; Larouche, S.; Lipworth, G.; Urzhumov, Y.; Reynolds, M.S. An analysis of beamed wireless power transfer in the Fresnel zone using a dynamic, metasurface aperture. *J. Appl. Phys.* **2017**, *121*, 014901. [CrossRef]
10. Liang, M.; Shemelya, C.; Macdonald, E.; Wicker, R.; Xin, H. 3-D Printed Microwave Patch Antenna via Fused Deposition Method and Ultrasonic Wire Mesh Embedding Technique. *IEEE Antennas Wirel. Propag. Lett.* **2015**, *14*, 1346–1349. [CrossRef]
11. Gillatt, B.T.; D'Auria, M.; Otter, W.J.; Ridler, N.M.; Lucyszyn, S. 3-D Printed Variable Phase Shifter. *IEEE Microw. Wirel. Compon. Lett.* **2016**, *26*, 822–824. [CrossRef]
12. Castro, A.T.; Babakhani, B.; Sharma, S.K. Design and development of a multimode waveguide corrugated horn antenna using 3D printing technology and its comparison with aluminium-based prototype. *IET Microw. Antennas Propag.* **2017**, *11*, 1977–1984. [CrossRef]
13. Zhang, S. Design and fabrication of 3D-printed planar Fresnel zone plate lens. *Electron. Lett.* **2016**, *52*, 833–835. [CrossRef]
14. Bukhari, S.S.; Whittow, W.; Zhang, S.; Vardaxoglou, J.; Whittow, W.; Vardaxoglou, J. Composite materials for microwave devices using additive manufacturing. *Electron. Lett.* **2016**, *52*, 832–833. [CrossRef]
15. Ehrenberg, I.M.; Sarma, S.E.; Wu, B.I. A three-dimensional self-supporting low loss microwave lens with a negative refractive index. *J. Appl. Phys.* **2012**, *112*, 073114. [CrossRef]
16. Yurduseven, O.; Flowers, P.; Ye, S.; Marks, D.L.; Gollub, J.N.; Fromenteze, T.; Wiley, B.J.; Smith, D.R. Computational microwave imaging using 3D printed conductive polymer frequency-diverse metasurface antennas. *IET Microw. Antennas Propag.* **2017**, *11*, 1962–1969. [CrossRef]
17. Xin, H.; Liang, M. 3-D-Printed Microwave and THz Devices Using Polymer Jetting Techniques. *Proc. IEEE* **2017**, *105*, 737–755. [CrossRef]
18. Yi, H.; Qu, S.W.; Ng, K.; Chan, C.H.; Bai, X. 3D Printed Millimeter-Wave and Terahertz Lenses with Fixed and Frequency Scanned Beam. *IEEE Trans. Antennas Propag.* **2016**, *64*, 442–449. [CrossRef]
19. Electrifi. Available online: https://www.multi3dllc.com (accessed on 29 August 2019).
20. Flowers, P.F.; Reyes, C.; Ye, S.; Kim, M.J.; Wiley, B.J. 3D printing electronic components and circuits with conductive thermoplastic filament. *Addit. Manuf.* **2017**, *18*, 156–163. [CrossRef]
21. Xie, Y.; Ye, S.; Reyes, C.; Sithikong, P.; Popa, B.-I.; Wiley, B.J.; Cummer, S.A. Microwave metamaterials made by fused deposition 3D printing of a highly conductive copper-based filament. *Appl. Phys. Lett.* **2017**, *110*, 181903. [CrossRef]
22. Kim, M.J.; Cruz, M.A.; Ye, S.; Gray, A.L.; Smith, G.L.; Lazarus, N.; Walker, C.J.; Sigmarsson, H.H.; Wiley, B.J. One-step electrodeposition of copper on conductive 3D printed objects. *Addit. Manuf.* **2019**, *27*, 318–326. [CrossRef]
23. Roy, S.; Qureshi, M.B.; Asif, S.; Braaten, B.D. A Model for 3D-Printed Microstrip Transmission Lines Using Conductive Electrifi Filament. In Proceedings of the IEEE International Symposium on Antennas and Propagation & USNC/URSI National Radio Science Meeting, San Diego, CA, USA, 9–14 July 2017; pp. 1099–1100.

24. Pizarro, F.; Salazar, R.; Rajo-Iglesias, E.; Rodríguez, M.; Fingerhuth, S.; Hermosilla, G. Parametric Study of 3D Additive Printing Parameters Using Conductive Filaments on Microwave Topologies. *IEEE Access* **2019**, *7*, 106814–106823. [CrossRef]
25. D-Bot Core-XY 3D Printer. Available online: http://www.thingiverse.com/thing:1001065 (accessed on 28 June 2019).
26. RepRap. Available online: https://reprap.org/wiki/RepRap (accessed on 28 August 2019).
27. Balanis, C.A. *Antenna Theory: Analysis and Design*, 3rd ed.; John Wiley & Sons: Hoboken, NJ, USA, 2005.
28. Bruker Dektak 150. Available online: https://www.brukersupport.com/ProductDetail/1135 (accessed on 24 June 2019).
29. Yurduseven, O.; Gollub, J.N.; Marks, D.L.; Smith, D.R. Alignment Correction for Antenna Scans in Imaging. In Proceedings of the IEEE International Symposium on Antennas and Propagation & USNC/URSI National Radio Science Meeting, San Diego, CA, USA, 9–14 July 2017; pp. 2381–2382.
30. Fromenteze, T.; Yurduseven, O.; Imani, M.F.; Gollub, J.; Decroze, C.; Carsenat, D.; Smith, D.R. Computational imaging using a mode-mixing cavity at microwave frequencies. *Appl. Phys. Lett.* **2015**, *106*, 194104. [CrossRef]
31. NSI-200v-3x3. Available online: https://www.nsi-mi.com/ (accessed on 29 August 2019).